A NOVEL GRAIN CONFIGURATION FOR DUAL THRUST SOLID ROCKET MOTOR USING TWO PROPELLANTS

Milan M. POPOVIĆ*[1,2], Milivoje M. POPOVIĆ[1], Predrag M. ELEK[2]

[1]EDePro, Kralja Milutina 33, Belgrade, Serbia
[2]University of Belgrade - Faculty of Mechanical Engineering, Kraljice Marije 16, Belgrade, Serbia
*Corresponding author; E-mail: mpopovicedepro@gmail.com

This paper presents the design of a propellant grain for a dual-thrust solid rocket motor, combining slotted and end-burner grain geometries with two propellants of different burn rates. This novel approach achieves a high thrust ratio between the two phases while ensuring nearly neutral burning throughout motor operation. Key performance parameters, such as chamber pressure and thrust, can be predicted analytically, with experimental tests demonstrating excellent agreement with theoretical models. The proposed design offers several advantages: neutral burning in both phases, a highly flexible and high thrust ratio, rapid pressure reduction during phase transition, minimal sliver formation, and quick motor extinction at the end of the second phase. Additionally, the use of thermoplastic propellant technology allows for the integration of multiple propellants within a single grain, providing versatility in using cylindrical-shaped grains for various applications.

Keywords : solid rocket motor, dual thrust, propellant grain design, grain burn-back analysis, thermoplastic composite propellant, rocket motor performance parameters, static rocket motor test

1 Introduction

Solid propellant rocket motors are used in different applications, going from tactical weapons to space missions [1]. In comparison to liquid propellant engines, solid rockets are usually relatively simpler, more reliable and require little servicing. However, they cannot be fully checked out prior to use and thrust cannot be randomly varied in flight.

For most types of solid propellant motors, the propellant grain typically constitutes 82% to 94% of the total motor mass, with the exeption of small and certain specialized motors. Many propellant grains have slots, grooves, holes, or other geometric features which alter the initial burning surface area. The burning surface area significantly influences the mass flow of combustion products and the resulting thrust. During the operation of solid rocket motor, propellant grain geometry changes and thus changing thrust profile. The process is often referred to as burn-back analysis of solid propellant grain [2-9].

The burning surface area is the most critical variable in calculating solid rocket propellant grain, as it directly determines the profile of thrust and pressure diagrams over time. For calculating pressure/thrust of rocket motor, the burning rate of propellant is an essential parameter that can be expressed by Saint Robert or

Vieille's law [10] :

$$r_0 = b \cdot p_o^n \tag{1}$$

where p_0 is the chamber pressure, and b and n are propellant specific parameters.

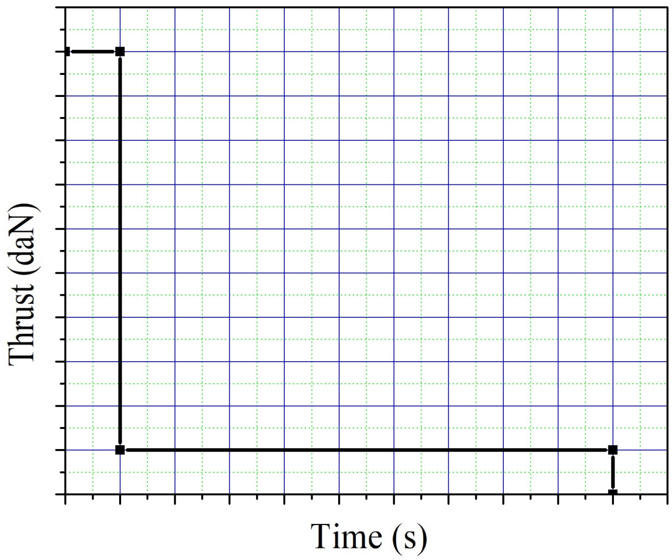

Figure 1. A typical thrust - time diagram requirement for a dual thrust solid rocket motor

Solid rocket motors are designed depending on mission requirements. In this paper, we will consider a dual thrust solid rocket motor (DTSRM) with a single propellant grain consisting of two propellants with different burning rates. A typical thrust-time diagram for a DTSRM is shown in Figure 1.

The thermoplastic propellant technology employed in this solution does not exhibit the inadequate mechanical properties suggested by Tsutsumi et al. [11], who noted that conventional thermoplastics have not been effectively utilized in composite propellants. Although the company EDePro has successfully implemented thermoplastic composite propellants in various applications [12], the specific solution considered here does not require exceptional mechanical properties, as the grain burns from its frontal surface. Consequently, the impact of mechanical properties on the propellant grain is minimal.

Naggar et al. [13] stated that old survey shows that 40% of 129 operational motors use star grain with a number of points ranging from 3 to 40. They used star shaped propellant grain for creating a dual phase rocket motor. By using thermoplastic propellant technology, a simple circular cylindrical propellant grain can be employed to mimic the characteristics of a star-shaped geometry, allowing us to achieve the benefits of neutral burning and other advantages associated with star shape. It is also possible to create a dual thrust motor with two propellants without a need to use a star shaped propellant grain. Compared to the solution presented in [13], thermoplastic technology enables the creation of a neutral second burning phase, as opposed to the slightly regressive burn profile produced by star-shaped propellant grain. Alazeezi et al. [14] conducted a mathematical analysis of a simplified scenario involving cylindrical propellant grains, utilizing two different propellants to facilitate a more efficient and straightforward burnback assessment. El-Nady et al. [15] proposed a solution involving dual-phase rocket motors that incorporate an intermediate nozzle. This interesting concept can be surpassed using a single propellant grain. The solution presented in this paper has a significantly higher volumetric efficiency factor and useful weight, as El-Nady's[15] dual-thrust rocket motor requires numerous additional components for proper operation.

Raza et al. [16] used a wagon wheel grain geometry to achievea dual thrust profile, similar to the proposed design in this paper. The present design is simpler due to the use of thermoplastic composite technology, as manufacturing a wagon wheel geometry would be more challenging without casting technology.

Papers of Gawad et al. [17] and Shakhar [18] also present solutions for propellant grains designed to achive dual thrust curves. However, their primary drawback is relativly low boost-to-sustain thrust ratio. This paper presents a case study to illustrate a novel, simple, and flexible design concept for the propellant charge of rocket engine with a dual-thrust curve. Following the Introduction, the second section thoroughly examines the geometry of the propellant charge in both operational phases. The third section (Results and Discussion) presents a detailed analysis of the computational results, comparing them with experimental data. The concluding section summarizes the study and highlights the key advantages of the proposed approach.

2 Propellant grain geometry

For achieving a typical required dual thrust-time diagram as in Figure 1, a simple two-component cylindrical propellant grain has been designed, Figure 2a.

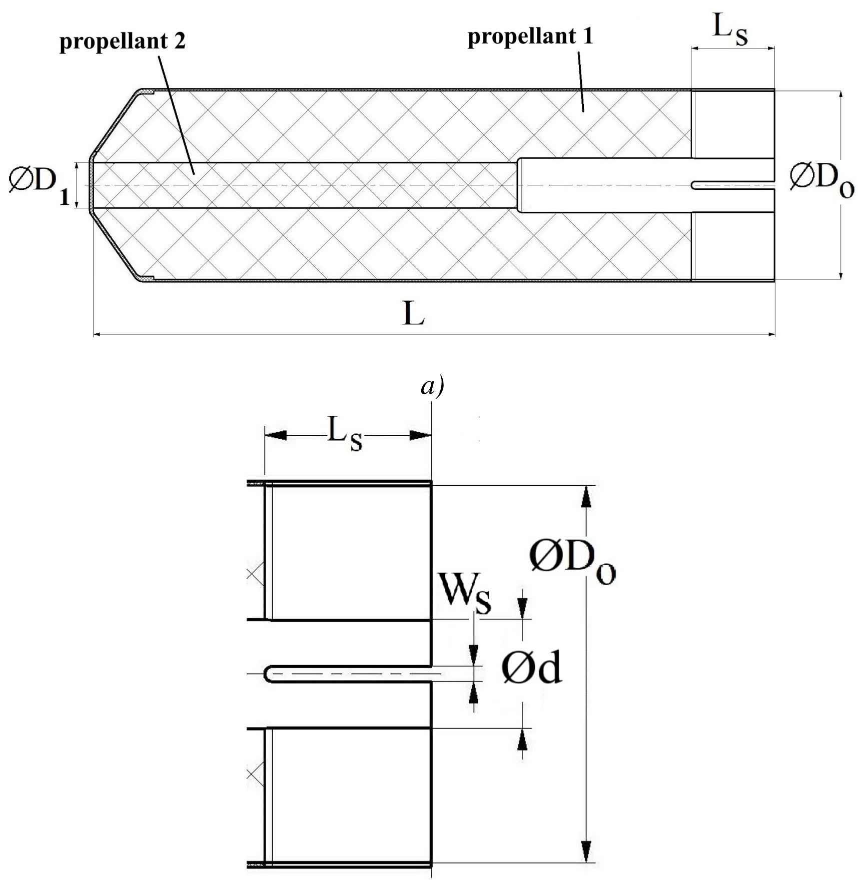

b)

Figure 2. a)Propellant grain drawing b) Grain geometry detail

Essentially, the first (booster) phase consists dominantly of the burning of a propellant 1 which has the cylindrical geometry with four slots. In the second (sustainer) phase, the combustion of both propellant 1 and 2 occurs with a specific end-burner (cigarette) geometry. The dimensions of the grain are optimized to provide neutral burning in both stages.

It should be noted that the burning rate of the propellant 2 should be higher than the propellant 1 burning rate. Also, both propellants start to burn when the motor is ignited, affecting the mass flow rates in both phases. The relevant dimensions of the grain are indicated in Figure 2a, as well as in the grain geometry detail as shown in Figure 2b.

2.1 Calculation of the burning surface area in the first phase

In the geometry used, four slots are responsible for the evolution of the burning surface area during the first phase. To determine the inner surface area of these slots, the complete inner and outer surface areas of each slot must be calculated, followed by subtracting the portion removed due to the curvature of the cylinder's outer diameter. This particular surface can be visualized in Figure 3.

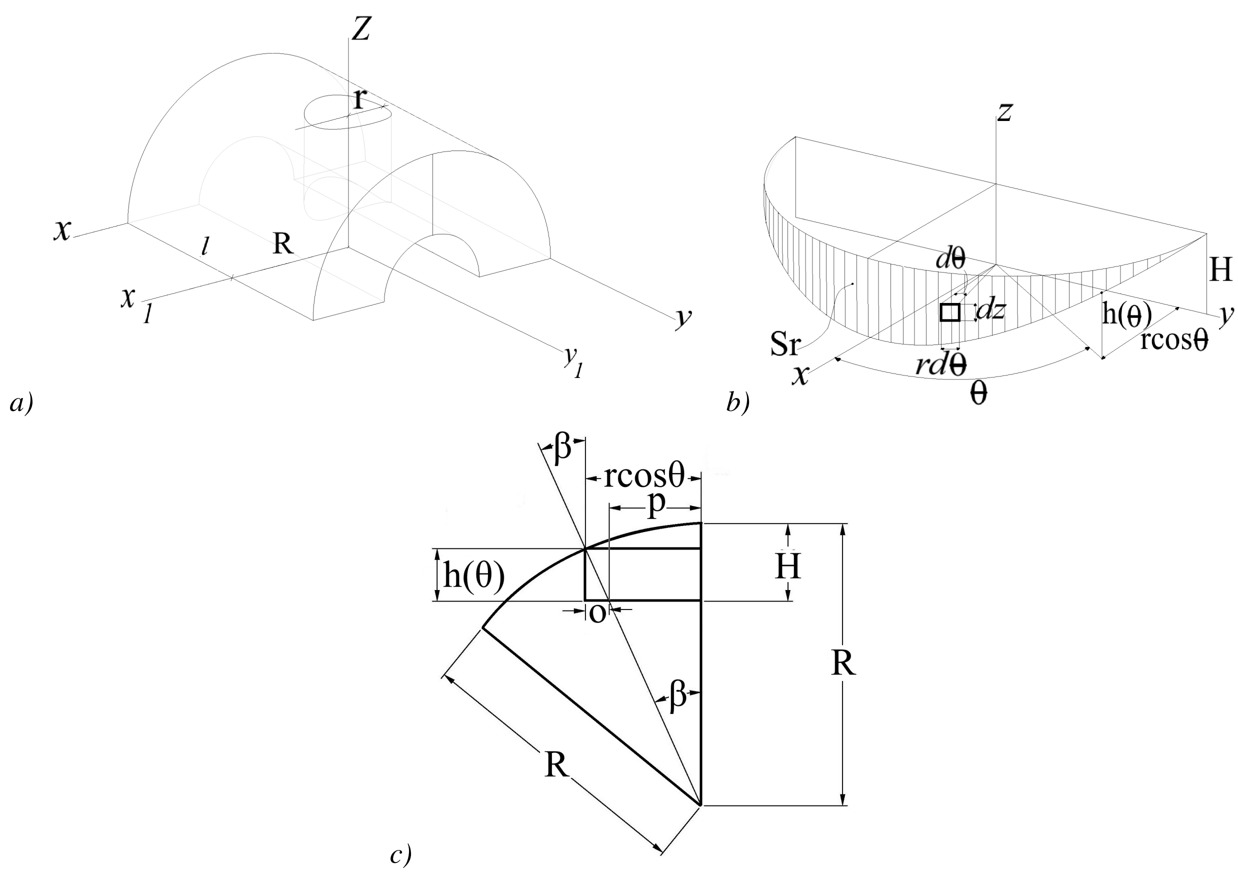

Figure 3 a) Slot burning surface detail; b) Segment area; c) Detail surface part

$$Sr = \int_{0}^{\frac{\pi}{2}} \int_{h(\theta)}^{H} r d\theta dz; Sr = \int_{0}^{\frac{\pi}{2}} r d\theta (H - h(\theta)) \tag{2}$$

where *Sr* is surface area of circural section, *H* is height of the segment, *R* is radius of propellant grain, *r* is slot radius shown in Figure 3. From the relation between geometric parameters can be found:

$$sin\beta = \frac{rcos\theta}{R} \tag{3}$$

and from there we get:

$$h(\theta) = H - R + \sqrt{R^2 - r^2cos^2\theta} \tag{4}$$

$$\int_0^{\frac{\pi}{2}} h(\theta)d\theta = \frac{\pi}{2}(H - R) + \int_0^{\frac{\pi}{2}} \sqrt{R^2 - r^2cos^2\theta}d\theta \tag{5}$$

The final expression Eq. (5) can only be integrated using numerical methods, having in mind the presence of an elliptic integral. To facilitate numerical calculations, we employed parametric CAD techniques to obtain the burning surface for both fast and slow burning propellants.

2.2 Link between grain geometry and propellant burning rates

Due to the different burning rates of the propellants, a cone with a constant angle α is maintained during the grain burning process. Burning rate factor is defined as:

$$\frac{r_2}{r_1} = k, k > 1 \tag{6}$$

where r_1 is burning rate of the propellant 1, and r_2 is burning rate of the propellant 2.

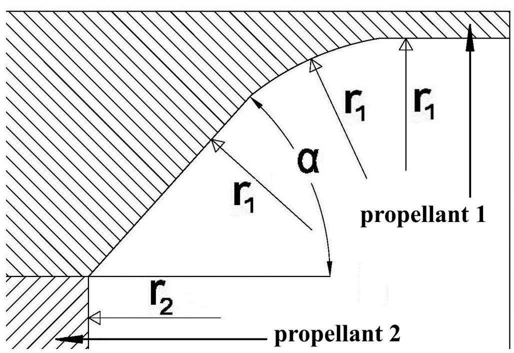

Figure 4. Angle of cone that is created by difference in burning rates of propellants

As shown in Figure 4 angle of cone, α depends on the burning rate factor according to:

$$sin\alpha = \frac{1}{k} = const. \tag{7}$$

The tapered cone with the same angle α (Figure 2a) at the end of the propellant grain is designed so that sliver that may appear at the end of the combustion process, is neutralized.

2.3 Mass flow rate in the second phase

Mass flow rate of combustion products (Figure 5) can be calculated as:

$$\dot{m} = \dot{V} \cdot \rho \tag{8}$$

where ρ is propellant density and $\dot{V}$ is volumetric flow rate. The mass flow rates of consumed propellants 1 and 2 are respectively:

$$\dot{m}_1 = r_1 \cdot \rho \cdot (D_o^2 - D_1^2) \cdot \frac{\pi}{4} \cdot \frac{1}{sin\alpha} \tag{9}$$

$$\dot{m}_2 = r_2 \cdot \rho \cdot D_1^2 \cdot \frac{\pi}{4} \tag{10}$$

where D_0 and D_1 are the outer diameters of propellant 1 and propellant 2, respectively (Figure 2a). The total mass flow rate is:

$$\dot{m} = \dot{m}_1 + \dot{m}_2 = \tag{11}$$
$$= r_1 \cdot \rho \cdot (D_o^2 - D_1^2) \cdot \frac{\pi}{4} \cdot \frac{1}{sin\alpha} + r_2 \cdot \rho \cdot D_1^2 \cdot \frac{\pi}{4}$$

and if we use the link between burning rates and the angle α, Eq. (6) and Eq. (7), then the total mass flow rate equals:

$$\dot{m} = r_2 \cdot \rho \cdot D_o^2 \cdot \frac{\pi}{4} \tag{12}$$

The presented equation indicates that the mass flow rate in the second phase is equivalent to the mass flow rate of a full diameter end-burner made from the propellant 2 only.

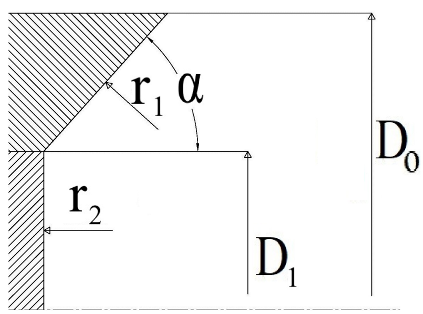

Figure 5. Propellant grain geometry in the second phase

3 Results and discussion

The simulation of combustion within a CAD model allows for the attainment of desired outcomes by utilizing specific dimensional ratios in relation to the diameter of the propellant grain. It is important to note that both propellants have the same density (ρ) as shown in Table 1. The relevant properties of both propellants are listed in Table 1. By utilizing thermoplastic composite technology and varying the granulation of ammonium perchlorate particle size, we can achieve identical propellant characteristics with varying burning rates. The objective of this design, as illustrated in Figure 1, was to attain a thrust ratio of boost to sustain phase exceeding 10, as well as a time ratio of 1:10 for each of these phases. This was accomplished through geometric optimization, as detailed in Table 2. All data are shown relative to the diameter of the propellant 1

(D_0). It is worth emphasizing that the proposed concept offers significant flexibility, allowing the thrust ratio and operation time in both booster and sustainer phases to be adjusted over a broad range.

Table 1. Characteristics of propellants:

Parameter	Fast-Burning Propellant	Slow-Burning Propellant
Density [kg/m^3]	1710.0	1710.0
Combustion Temperature [K]	2611.3	2611.3
Adiabatic constant	1.1925	1.1925
Molar mass [g/mol]	25.596	25.596
Burning rate exponential coefficient n	0.42	0.42
Burning rate liear coefficient b [$ms^{-1}Pa^{-n}$]	0.0000198	0.0000165

Table 2. Dimensions relative to D_0:

Dimension	Dimension relative to D_0
Diameter of propellant 2 (D_1)	D_1 = 0.24 D_0
Hole diameter (d)	d= 0.29 D_0
Hole length (L_0)	L_0=1.33 D_0
Slot length (L_S)	L_S=0.43 D_0
Slot width (W_S)	W_S=0.04 D_0
Total propellant length (L)	L= 3.54 D_0
Throat diameter (d_t)	d_t =0.11 D_0

The burning surface area was calculated and optimized using the CAD model created in CREO Parametric 4.0, which involved the analysis of both propellants. Figure 6 illustrates the simulation of the burning surfaces of both propellants during complete operation of the rocket motor. In Figure 7, the burning surface of the initial phase of the propellant 1 is illustrated, highlighting that the predominant section contains slots. Figure 8 shows the burning surface of the second phase for the propellant 1. Figure 9 depicts the first and second phases of the propellant 2 and it is evident that the burning surface remains consistent for the propellant 2.

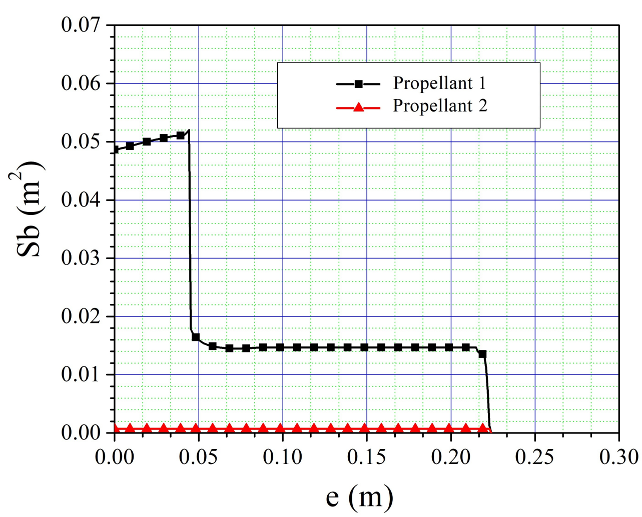

Figure 6. Burning surface area of the propellants 1 and 2 as a function of burned web thickness

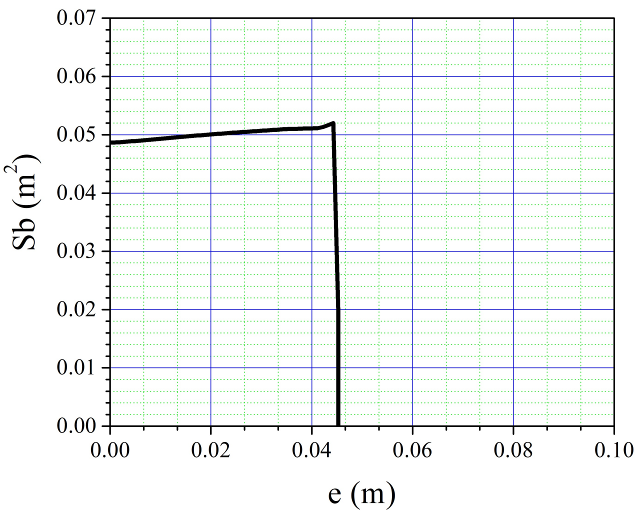

Figure 7. Burning surface of first phase, propellant 1

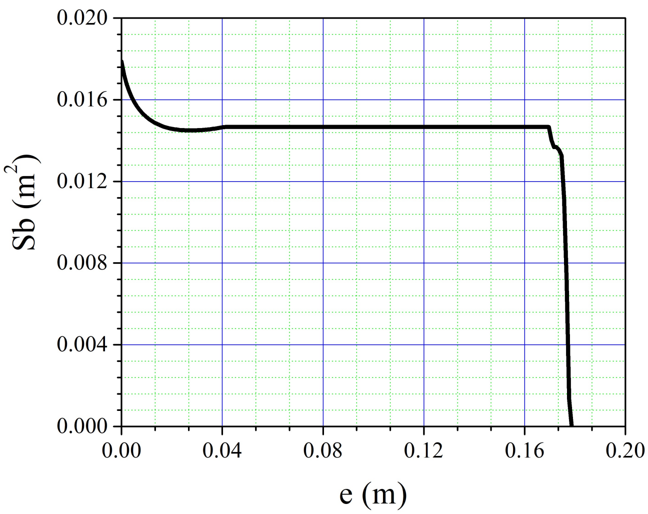

Figure 8. Burning surface of second phase, propellant 1

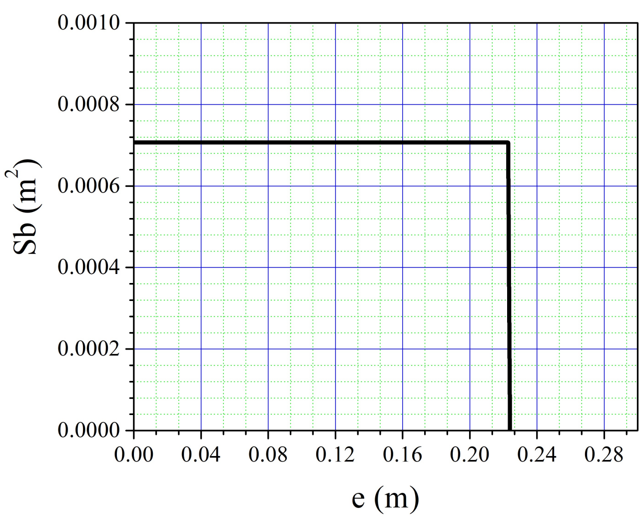

Figure 9. Burning surface of propellant 2

Characteristic velocity c*, the main energetic property of a propellant, is defined as the product of chamber pressure p_0 and nozzle throat area A_t divided by the propellant mass flow rate $\dot{m}$ and can be expressed in the form:

$$c^* = \frac{p_0 A_t}{\dot{m}} \tag{13}$$

Balancing the mass flow rate of the generated gas Eq. (8) and the mass flow rate through the nozzle Eq. (13) we can obtain the equilibrium chamber pressure :

$$p_0 = (b\rho c^* \frac{S_b}{A_t})^{\frac{1}{1-n}} \tag{14}$$

The motor thrust can be calculated from:

$$F = c_F p_0 A_t \tag{15}$$

where c_F is the thrust coefficient, the main property of the nozzle. The interior ballistics of the rocket motor were calculated using a simple mathematical simulation made in MATLAB and then compared to the corresponding test results.

a)

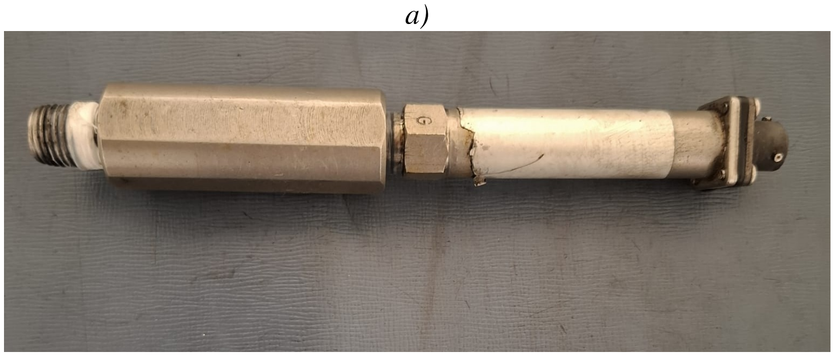

b)

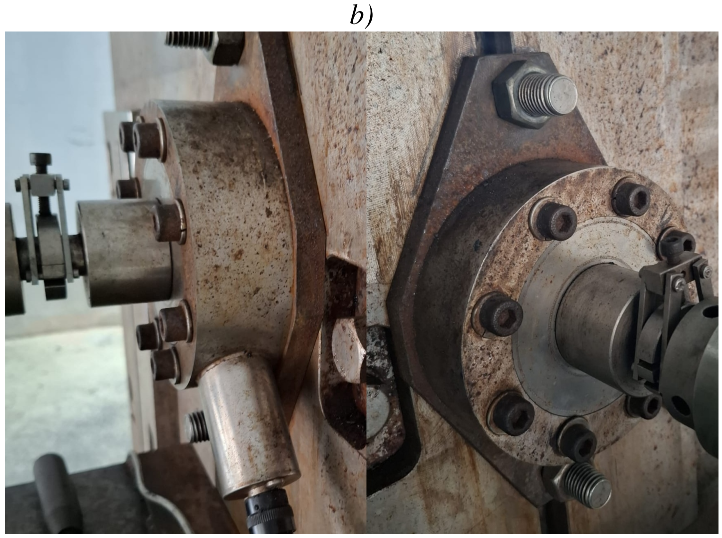

Figure 10. a) Pressure sensor, b) Thrust sensor

Test measurements were captured using a data acquisition system. The pressure measurement was conducted with Omega PX613 pressure transducer, capable of measuring pressures up to 5000 psi, equivalent to approximately 345 bar. For force measurement, the Omega LCHD-TP263 load cell was utilized, which can measure force up to 5000 pounds, roughly translating to 22 250 N (Figure 10).
The thrust coefficient is evaluated continuously and varies over the course of the rocket motor's operation. Since the same nozzle is used in both phases, the thrust coefficient is directly influenced by chamber pressure. During the boost phase, it is approximately around 1.55 , while in the sustain phase it remains approximately at around 1.40, however when thrust coefficient is calculated accounting for thrust losses in the nozzle, values of around 1.49 for boost phase and around 1.35 for the sustainer phase.

Theoretical prediction of the chamber pressure vs. time along with experimental data is presented in Figure 11. A similar diagram which represents both calculated and measured time dependance of the motor thrust is given in Figure 12. The analytical and experimental results show a high degree of agreement. However, the discrepancy observed toward the end of the initial phase is attributed to throat erosion, which is not fully captured in the simulation. This limitation arises from the use of a simple linear erosion model, which does not accurately represent the nonlinear behavior observed under real conditions.

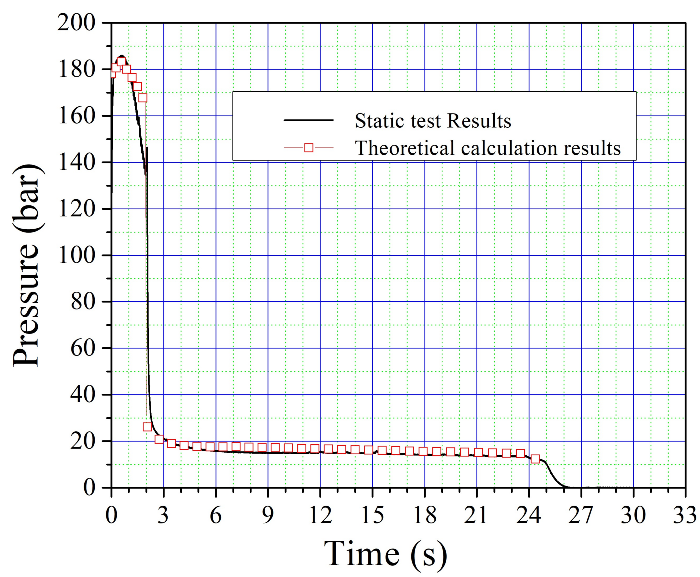

Figure 11. Analytically and experimentally obtained chamber pressure vs. time diagrams

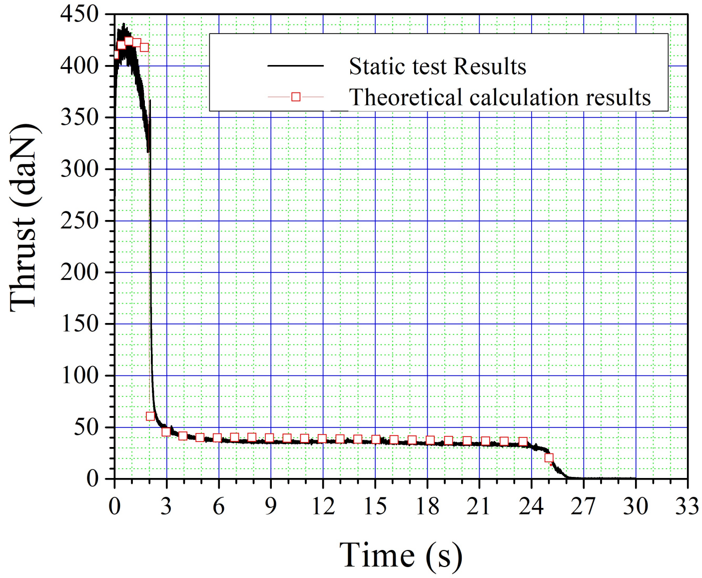

Figure 12. Comparison of theoretical and experimental values of motor thrust vs. time

The usage of two propellants provides the advantage of complete control over the thrust curve. This allows for a very fast transition from one phase to another, with the removal of any slivers. The removal of the sliver at the end of the diagram can be achieved through geometry design.

During the second phase, it is necessary to account for the erosion of the throat that occurred during the first phase. The extent of erosion is dependent on the material of the throat and the type of propellant used. In our specific case, where graphite was utilized as the throat material, we experimentaly observed erosion of approximately 4.3% of the throat diameter. To achieve optimal performance, a nozzle expansion ratio of 3.5 was adopted, being close to the adapted nozzle during the second phase of motor operation.

Frames captured during the static test, as depicted in Figure 13, clearly reveal a noticeable difference between the first and second phases of rocket motor operation, even when viewed on camera from inside the test box.

a)

b)

Figure 13. a) First (boost) phase of motor operation; b) Second (sustain) phase of motor operation, (Frames captured from video footage of static test)

4 Conclusion

The combination of slotted and end-burner grain geometry, using two propellants with different burning rates presents a new way of designing a two phase solid rocket motor with high thrust ratio of two phases. It is shown that the design ensures practically neutral burning in both phases of the motor operation. The main performance parameters- the chamber pressure and thrust- can be analytically predicted. The experimental test was performed, demonstrating excellent agreement with theoretical prediction.The suggested geometric configuration enables: approximately neutral burning in both the first and second phases, a very high thrust ratio, a fast reduction of pressure in transition from the first to the second phase, a minimization of slivers, and a fast motor extinction that marks the end of the second phase. The application of thermoplastic propellant with corresponding technology enables the incorporation of multiple propellants within a single propellant grain, thereby enabling the user to employ a cylindrical-shaped propellant grain for a variety of applications.

Nomenclature

D_o - Outer diameter of propellant grain
d - Inner diamatar of propellant grain
L - Total lenght of propellant grain
L_d - Hole lenght
L_s - Slot lenght
W_s - Slot width
D_1 - Diameter of propellant 2
k - Burning area ratio
r_1 - Burning rate of the propellant 1
r_2 - Burning rate of the propellant 2
$\dot{m}_1$ - Mass flow rate of the propellant 1
$\dot{m}_2$ - Mass flow rate of the propellant 2
ρ - Density of propellants
α - Angle of cone created due to difference in burning rates of propellants
$\dot{V}$ - Volumetric flow rate
S_b - Burning surface of propellant grain
S_{b1} - Burning surface of the propellant 1
S_{b2} - Burning surface of the propellant 2

5 Literature

[1] Fabignon, Y., "Recent Advances in Research on Solid Rocket Propulsion", AerospaceLab,11, (2016) pp. 1-15

[2] Reddy, K.O., Pandey, K. M., "Burnback Analysis of 3-D Star Grain Solid Propellant", International Journal of Advanced Trends in Computer Science and Engineering, 2 (2013), 1, pp. 215-223

[3] Oh, S. H., "Study on Solid Propellant Grain Burn-back Analysis Applying Face Offsetting Method", Journal of the Korean Society of Propulsion Engineers, 23 (2019), 4, pp. 81-91

[4] Puskulcu, G., Ulas, A., "3-D Grain Burnback Analysis of Solid Propellant Rocket Motors: Part 1 Ballistic Motor Test", Aerospace Science and Technology, 12 (2008), 8, pp. 579-584

[5] Puskulcu, G., Ulas, A., "3-D Grain Burnback Analysis of Solid Propellant Rocket Motors: Part 2 Modelling and Simulations", Aerospace Science and Technology, 12 (2008), 8, pp. 585-591

[6] Sutton, G. P., Biblarz, O. "Rocket Propulsion Elements, Seventh Ed", A Wiley Interscience Publication of John Wiley and Sons, INC., 11 (2001), pp. 1-15

[7] Sforza, P.M.: Chapter 12 - Solid Propellant Rocket Motors, in: Theory of Aerospace Propulsion, (Ed. P. M. Sforza), Butterworth-Heinemann, 2017, pp. 617-668.

[8] Heister, S.D., Anderson, W. E., Pourpoint, T. L., Cassady, R. J. (2019). Chapter 7 - Solid Rocket Motors, in : Rocket Propulsion, (Ed. S. D. Heister et al.), Cambridge University Press, 2019, pp 229-281.

[9] Tizon, J. M. , "Burn-back Analysis of Solid Propellant Rocket Motors", Departamento de Mecanica De Fluidos Y Propulsion Aeroespecial, ETSIAE, Universidad Politecnica de Madrid (UPM) , Madrid, Spain (2023)

[10] Gossant, B., "Solid Propellant Combustion and Internal Ballistics", Sollid Rocket Propulsion Technology (Ed.A.Davenas), Peramon Press, New York, USA (1993)

[11] Tsutsumi, A., Hori, K., Morita, Y., Akiba, R., Hasagawa, H., Sasaki, K., Kato, N., : "A Study on Low Melting Point Thermoplastic Solid Propellant", Japan Society for Aeronautical and Space Science and ISTIS, 10 (2012), ists 28, pp. 85-88

[12] www.edepro.com/products-and-services/rocket-propulsion, retrieved 22.03.2025.

[13] El-Naggar, M., Belal, H., Abdalla, H. M., : "Design of a Dual Thrust Solid Motor using Star Grain", AIAA Propulsion and Energy Forum 19-22 August 2019, Indianapolis, IN. AIAA Propulsion and Energy 2019 Forum (2019)

[14] M. Alazeezi, N. Popovic, P. Elek :"Two-component propellant grain for rocket motor: Combustion analysis and geometric optimization", Thermal Science (2022), 26, 2B, pp. 1567-1578

[15] AM El-Nady, MYM Ahmed, MA El-Senbawy, AM Sarhan :"Experimental and theoretical study on a dual-thrust motor with subsonic intermediate nozzle", Institution of Mechanical Engineers Part G:, Journal of Aerospace Engineering (2017) pp. 1-9

[16] Raza, M. A., Liang, W., : "Design and Optimization of 3D Wagon Wheel Grain for Dual Thrust Solid Rocket Motors", Propellants, Explosives, Pyrotechnics, 38 (2012) 1, pp 67-74

[17] Gawad, A. R. A., Ahmed, M. Y. M., Abdalla, H. M., & El-Senbawy, M. A. (2016). Pressure Profile Prediction of Dual-Thrust Rocket Motors under Uncertainties. Propellants, Explosives, Pyrotechnics, 41 (6), 965-971.

[18] Shekhar, H.: Burn-back Equations for High Volumetric Loading Single-grain Dual-thrust Rocket Pro-

pellant Configuration, Defense Science Journal (2011), Vol.61, No. 2, pp. 165-170.

Submitted: 30.12.2024.
Revised: 25.03.2025.
Accepted: 14.04.2025.